Effect of Alkyl Length of Peptide−Polymer Amphiphile on Cargo Encapsulation Stability and Pharmacokinetics of 3-Helix Micelles

Nikhil Dube,[†] Jai W. Seo,[‡] He Dong,[†] Jessica Y. Shu,[†] Reidar Lund,[†] Lisa M. Mahakian,[‡] Katherine W. Ferrara,[‡] and Ting Xu*[†,§,‖]

[†]Department of Materials Science & Engineering and [§]Department of Chemistry, University of California, Berkeley, California 94720, United States

[‡]Department of Biomedical Engineering, University of California, Davis, California 95616, United States

[‖]Materials Science Division, Lawrence Berkeley National Laboratory, Berkeley, California 94720, United States

S Supporting Information

ABSTRACT: 3-Helix micelles have demonstrated excellent *in vitro* and *in vivo* stability. Previous studies showed that the unique design of the peptide−polymer conjugate based on protein tertiary structure as the headgroup is the main design factor to achieve high kinetic stability. In this contribution, using amphiphiles with different alkyl tails, namely, C16 and C18, we quantified the effect of alkyl length on the stability of 3-helix micelles to delineate the contribution of the micellar core and shell on the micelle stability. Both amphiphiles form well-defined micelles, <20 nm in size, and show good stability, which can be attributed to the headgroup design. C18-micelles exhibit slightly higher kinetic stability in the presence of serum proteins at 37 °C, where the rate constant of subunit exchange is 0.20 h^{-1} for C18-micelles vs 0.22 h^{-1} for C16-micelles. The diffusion constant for drug release from C18-micelles is approximately half of that for C16-micelles. The

differences between the two micelles are significantly more pronounced in terms of *in vivo* stability and extent of tumor accumulation. C18-micelles exhibit significantly longer blood circulation time of 29.5 h, whereas C16-micelles have a circulation time of 16.1 h. The extent of tumor accumulation at 48 h after injection is ∼43% higher for C18-micelles. The present studies underscore the importance of core composition on the biological behavior of 3-helix micelles. The quantification of the effect of this key design parameter on the stability of 3-helix micelles provides important guidelines for carrier selection and use in complex environment.
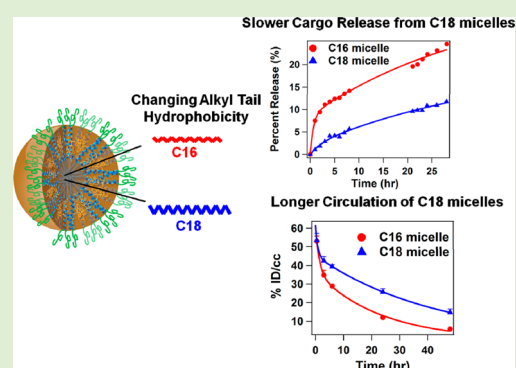
INTRODUCTION

Micellar nanoparticles have been studied extensively for use as nanocarriers for imaging and drug delivery.[1−14] Control over stability of micelles is critical to optimize their pharmacokinetics, biodistribution, and clearance mechanism.[15−18] Fundamental studies focused on the molecular design parameters that can be used to tune micelle stability have been instrumental in generating stable polymeric nanocarriers in the size range of 50−150 nm.[19−25] Recent studies have established advantages of smaller nanocarriers in the size range of 10−30 nm, in terms of favorable transport properties in blood circulation, facile extravasation from vasculature to tumor tissues, and homogeneous distribution in tumor.[14,18,26,27] We recently reported the design of 15 nm 3-helix micelles based on an amphiphile with headgroup of PEG attached to the exterior of a coiled-coil 3-helix bundle.[18] Intravenous administration of doxorubicin (DOX) loaded 3-helix micelles in mice indicated increased tumor accumulation with extended drug half-life and reduced side effects.[14]

The unique design of the 3-helix micelle headgroup, consisting of a polymer-conjugated coiled-coil helix bundle,

imparts the micelles with excellent kinetic stability.[28] The protein tertiary structure in the headgroup allows entropic repulsions between the polymer chains that slows the subunit exchange and stabilizes 3-helix micelles.[28] Studies of PEG-lipid micelles have shown that increasing the length of the alkyl tails leads to decreased *in vitro* subunit exchange and higher stability.[29] However, the stability of 3-helix micelles as a function of tail hydrophobicity has not been quantified. These quantitative studies should provide critical guidelines to design and formulate 3-helix micelles with tunable stability for a range of applications for nanocarriers. In addition to understanding the effect of the alkyl tail on the *in vitro* stability of 3-helix micelles, it is equally, if not more, critical to evaluate the effect of relevant design parameters on *in vivo* stability of micelles to establish if the results from *in vitro* analytical characterization can be used as a guideline for *in vivo* studies and to predict micelle stability in biological environments.
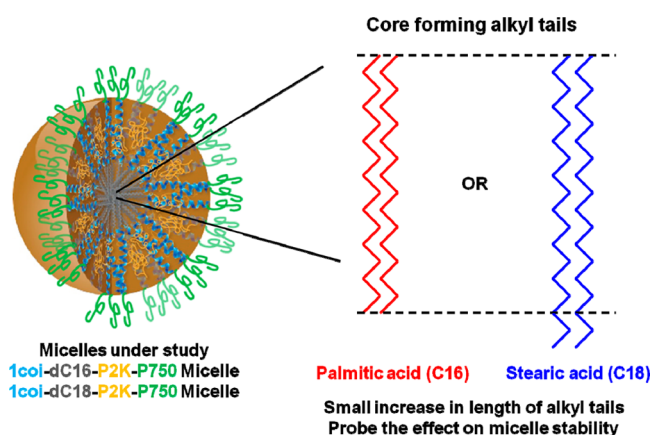
Our initial design consists of an amphiphile comprising a coiled-coil peptide (1coi) conjugated to stearic acid (C18) at the N-terminus and PEG-2000 Da (P2K) at the middle of the peptide backbone, which is called "1coi-dC18-P2K". Conjugation of a PEG-750 Da (P750) chain at the C-terminus results in "1coi-dC18-P2K-P750", and micelles based on this amphiphile were used for *in vivo* evaluation.[18] The physical characterization of kinetic stability of 3-helix micelles was performed using micelles assembled from "1coi-dC16-P2K", without P750 chains required for stealth layer, in our earlier work.[28] Here, we present a systematic investigation of the effect of the core forming alkyl chains on the size, core packing, drug release kinetics, *in vitro* and *in vivo* stability, and biodistribution of 3-helix micelles. In this study, amphiphiles have identical headgroups based on peptide–PEG conjugate 1coi-P2K-P750, and the hydrophobic alkyl tails are C16 and C18, respectively (Scheme 1), which allows evaluation of the exclusive effect of

blood circulation time of 3-helix micelles for different biological applications.

■ EXPERIMENTAL SECTION

Synthesis of Peptide–Polymer Conjugate. The design of the two amphiphilic conjugates is based on a 3-helix bundle peptide designed *de novo*, 1coi (EVEALEKKVAALECKKVQALEKKVEALE-HGW).[33] Aliphatic tails of palmitic acid (C16) and stearic acid (C18) were conjugated to the N-terminus of the peptide to investigate the effect of hydrophobicity of alkyl tails on assembly and stability of C16- and C18-micelles. The details of the materials and the synthesis of amphiphilic peptide–polymer conjugate have been described previously.[18] Conjugates were purified by reverse-phase high pressure liquid chromatography (RP-HPLC). 1coi-dC16-P2K-P750 conjugates were eluted with a linear AB gradient, where solvent A consisted of water plus 0.1% (v/v) TFA and solvent B consisted of acetonitrile plus 0.1% (v/v) TFA. For 1coi-dC18-P2K-P750, solvent B was isopropanol plus 0.1% (v/v) TFA. A linear gradient of 30% to 100% B over 30 min was used for both conjugates, with typical elution of amphiphiles at ~85% B.

Biophysical Characterization of C16- and C18-Micelles. C16- and C18-micelles were prepared by direct dissolution of the lyophilized powder in phosphate buffer (25 mM, pH 7.4). The solutions were annealed at 70 °C for an hour to allow equilibration of micelle assembly. The annealed solutions were cooled down to room temperature before use. Dynamic light scattering (DLS) size measurements were made on a Malvern Zetasizer Nano-ZS with a 633 nm laser and a scattering angle of 17°. Size exclusion chromatography (SEC) was carried out on a BioSep-SEC-S 4000 column (Phenomenex), with a flow rate of 1 mL/min, and 25 mM phosphate buffer, pH 7.4, was used as the elution solvent. Small angle X-ray scattering (SAXS) was carried out at beamline 7.3.3 at the Advanced Light Source, Lawrence Berkeley National Laboratory. Details on the sample preparation and data analysis for SAXS measurements can be found in our earlier work.[28] Circular dichroism (CD) measurements were made were made on a Jasco J810 spectropolarimeter from 260 to 190 at 0.2 nm intervals, a rate of a 100 nm/min, a response time of 4 s, and a bandwidth of 1 nm. Differential scanning calorimetry (DSC) was performed on a VP-MicroCal (GE), as temperature was increased from 5 to 60 °C at a rate of 1 °C/min. DSC thermograms were obtained after concentration normalization and baseline correction with Origin software provided by MicroCal. The enthalpy change associated with alkyl chain phase transition was calculated by using the area under the curve function in Igor Pro 6. A concentration of 2 mg/mL was used for both CD and DSC measurements. The *in vitro* stability of micelles in serum albumin was studied by Förster resonance energy transfer (FRET) from micelle-encapsulated donor/acceptor dyes, as described previously.[18] A lipophilic FRET pair, 3,3′-dioctadecyloxacarbocyanine perchlorate (DiO, donor) and 1,1′-dioctadecyl-3,3,3′,3′-tetramethylindocarbocyanine perchlorate (DiI, acceptor), were used to measure the energy transfer upon mixing. The emission spectra were recorded in the range of 475 to 650 nm for 12 h with excitation wavelength at 450 nm. The efficiency of energy transfer between the dyes is characterized by FRET ratio, defined as $I_{565}/(I_{565} + I_{505})$, where I is fluorescence intensity at the respective wavelength.

Loading and Release of DOX from Micelles. The loading of DOX in 3-helix micelles was performed by the thin film hydration method as described in earlier work.[14] The release profiles of DOX from micelles were studied using the dialysis bag technique at 37 °C. The solution of DOX-loaded micelles (3 mg/mL, 2 mL) was placed in a dialysis bag (Spectrum Laboratories, MWCO 3500 Da). The dialysis bag was immersed in 500 mL of PBS solution (25 mM, pH 7.4) in a glass beaker, which was stirred at 600 rpm. Ten microliters of solution was drawn from a dialysis bag at desired time intervals and the drug concentration was analyzed using RP-HPLC. DOX release profiles were fit to a Higuchi model for diffusive release, described by $Q = 2C_o(Dt/\pi)^{1/2}$, where Q is the amount of drug released per unit area, C_o is the initial drug concentration in the micelle, t is the time in seconds,

Scheme 1. Schematics of 3-Helix Micelle Depicting the Choice of Two Alkyl Tails with Different Chain Length and Hydrophobicity[a]

[a]Quantification of the effects of the alkyl tail on *in vitro* and *in vivo* stability of 3-helix micelles was performed to establish the significance of core composition for design of nanocarriers with tunable stability.

alkyl tails on 3-helix micelle stability. We denote the micelles as "C16-micelle" and "C18-micelle" The differences between the two micelles in terms of their *in vitro* stability and cargo release kinetics are minimal. However, the difference in blood circulation time of the two micelles is more pronounced than that shown by *in vitro* studies. These results demonstrate the importance of enthalpic contributions from alkyl chains in the micellar core, in addition to the entropic repulsion in the headgroup, toward micelle stability, most notably in biological conditions *in vivo*.

The desirable circulation times of nanoparticles vary for different applications. For example, faster accumulation at the target site, along with rapid blood clearance, is advantageous for imaging with high contrast and a high signal-to-noise ratio. On the other hand, longer circulation times would result in increased exposure of the nanocarrier to the vasculature, and hence would be useful for targeting blood vessels and other components in vasculature. Nanocarriers with longer blood circulation time are also attractive for the passive targeting of tumor tissue.[30−32] The quantitative evaluations in this study provide a useful guideline to tailor the *in vivo* stability and the

and D is the apparent diffusion constant.[34] The Higuchi equation can be rearranged to obtain fractional drug release, f, as $f = kt^{1/2}$, with the Higuchi rate constant, $k = (36D/\pi R^2)^{1/2}$, where R is the radius of the micelle.

PET Imaging and Biodistribution. All animal studies were conducted under a protocol approved by the University of California, Davis, Animal Care and Use Committee. $^{64}CuCl_2$ was purchased from Washington University (St Louis, MO). The details of the synthesis of radiolabeled micelles and PET imaging scans are described in previous work.[18] In brief, the pharmacokinetics and in vivo biodistribution of C16- and C18-micelles were studied by positron emission tomography (PET) and an automatic gamma counter (PerkinElmer, CT), respectively, after intravenous administration of the micellar solution to female FVB mice ($n = 6$ for C18-micelles, (371 ± 107 μCi and 0.68 ± 0.15 mg per mouse) and $n = 4$ for C16-micelles, (407 ± 9 μCi and 0.69 ± 0.008 mg/mouse) bearing new deletion mutant (NDL)[35,36] tumors implanted bilaterally within the mammary fat pads. All PET images and the organ distribution of ^{64}Cu-labeled micelles presented here have been decay corrected.

RESULTS AND DISCUSSION

The synthesis and characterization of 1coi-dC18-P2K-P750 has been described previously.[18] Mass spectroscopy of 1coi-dC16-P2K-P750 (Supporting Information Figure SI1) shows average molecular weight of 7150 Da, consistent with the theoretical weight of 7153 Da. Both amphiphiles form micelles with a uniform size distribution as confirmed by DLS and SEC (Supporting Information Figure SI2). There are no adverse effects of conjugation of C16 and C18 chains on the secondary and tertiary structure of 1coi, with peptide helicity ~82% in both amphiphiles, maintained at the level similar to peptide alone (Supporting Information Figure SI3). The peptide structure is stabilized after conjugation of hydrophobic alkyl tails, as observed previously[37,38] (Supporting Information Figure SI4). Figure 1 shows the SAXS profiles of both micelles in solution. Using a core–shell spherical model, the radius of
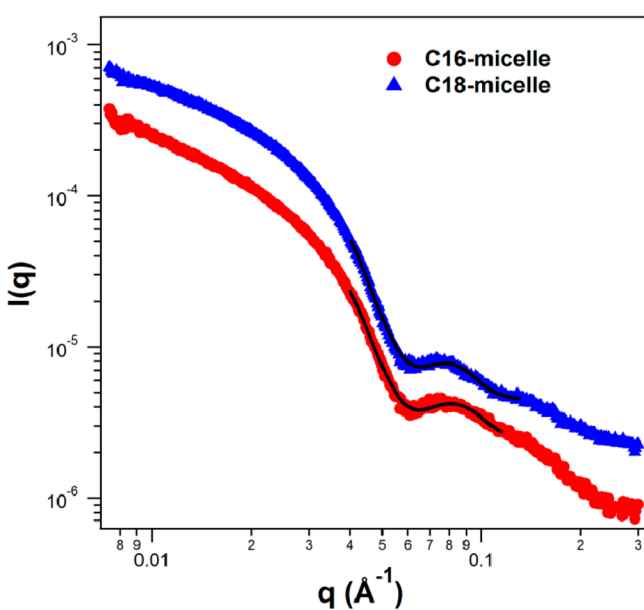
Figure 1. SAXS of C16- and C18-micelles dissolved in phosphate buffer (25 mM, pH 7.4), both at a concentration of 5 mg/mL. Fitting of the data (solid lines) in a q range of 0.03–0.1 Å^{-1} to a core–shell spherical form factor yields core radii of ~2.8 nm for C16, and ~3 nm for C18-micelles. Shell thickness is calculated to be ~5.7 nm for both micelles.

the core of C16-micelles is ~2.8 nm and thickness of shell is ~5.7 nm, giving an overall diameter of ~17 nm. For C18-micelles, the core radius is ~3.0 nm with shell thickness ~5.8 nm, which corresponds to diameter of ~17.6 nm. The alkyl chain length has minimal, if any, effect on the hydrodynamic size of micelles and the structure and thermal stability of the peptide in the headgroup. Any differences in terms of in vitro stability, pharmacokinetics, and biodistribution observed between the two micelles can be safely attributed to the effect of core chain hydrophobicity. Hence, 3-helix micelles provide a good model system to understand the effect of a relevant design parameter (alkyl chain length in the present study), exclusively on the biological stability of smaller particles, <20 nm in size, intended for nanocarrier applications.

DSC was performed to characterize the packing of alkyl chains in the micelle core. Both micelles show an endothermic phase transition, consistent with a change in alkyl chain packing in the core of micelles (Figure 2). For C16-micelles, the
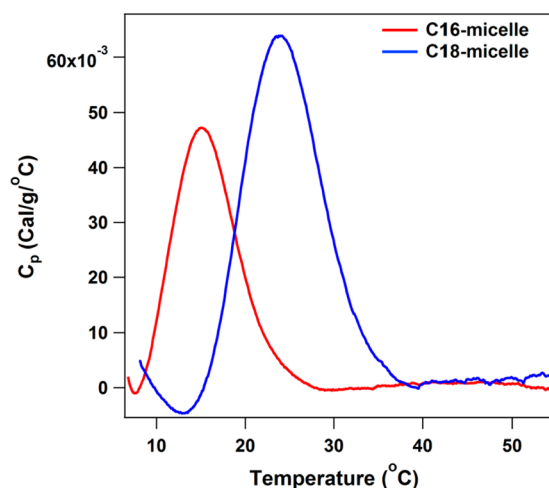
Figure 2. DSC thermograms for C16 and C18-micelles dissolved in phosphate buffer (25 mM, pH 7.4), both at concentration of 2 mg/mL. The phase transition temperature for C16-micelle core is 15 °C, and that for C18-micelle core is 24 °C. The higher transition temperature for C18-micelles is consistent with higher hydrophobicity of C18 alkyl chains.

transition temperature is 15 °C with the enthalpy associated with the phase transition being ~0.408 cal/g. For C18-micelles, the transition temperature is 24 °C, and the enthalpy associated with the transition is ~0.674 cal/g. The transition enthalpies for both chains in the micelle core are significantly smaller compared to that in bulk and can be attributed to the packing of alkyl tails in a curved geometry in micelle core. These results are in agreement with previous studies, where an increase in the chain length of the hydrophobic tails leads to an increase in the melting temperature and transition enthalpy of the alkyl chains in hydrophobic core of micelles.[39−41]

The effect of the alkyl tail length on the stability of 3-helix micelles at physiological temperature (37 °C) was studied to estimate their suitability in vivo. Quantification of the in vitro half-life of 3-helix micelles was performed by monitoring the changes in FRET from C16- and C18-micelles coencapsulated with donor−acceptor pair (DiO−DiI) dyes. As shown in Figure 3A and 3B, the emission spectra show a major peak at 565 nm and a minor peak at 505 nm. The increase in emission intensity at 505 nm as a function of time indicates subunit exchange and
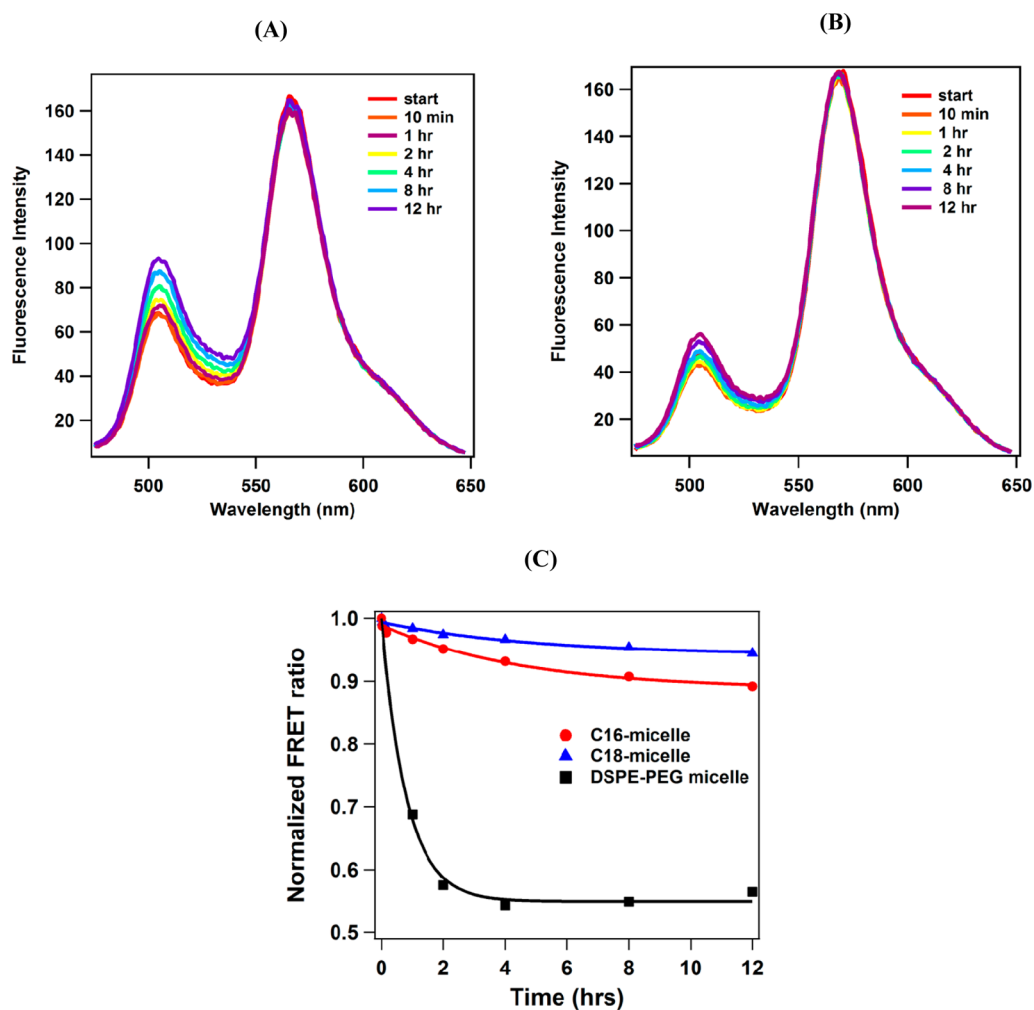
(A)

(B)

(C)

Figure 3. Emission spectra of (A) C16 (B) C18-micelles encapsulated with donor/acceptor pair of FRET dyes. Micelles are dissolved in phosphate buffer (25 mM, pH 7.4) at a concentration of 0.2 mg/mL. The changes in fluorescence intensity are monitored for 12 h in the presence of serum albumin (50 mg/mL) at 37 °C. The excitation wavelength was 450 nm and the emission spectra are recorded from 475 to 650 nm. (C) Plot of normalized FRET ratio as a function of time for different micelles. The solid lines are the exponential fits to the decay observed. The fitting of the data gives decay constant (η), which is an indicator of micelle stability. The values of η obtained by fitting for different micelles are 0.22 h^{-1} for C16-micelles; 0.20 h^{-1} for C18-micelles; 1.24 h^{-1} for DSPE-PEG micelles.

release of FRET dyes from the micelle. Figure 3C shows the normalized FRET ratio of $I_{565}/(I_{565} + I_{505})$ for the two micelles as a function of time. After 12 h, FRET ratios for C16- and C18-micelles are 0.892 and 0.945, respectively. The change of the FRET ratio with time, fitted to an exponential decay, gives the decay rate constants (η), which are 0.22 h^{-1} for C16-micelle and 0.20 h^{-1} for C18-micelle, respectively. The half-life ($t_{1/2}$) corresponding to the first-order decay constant is 3.15 and 3.46 h for C16- and C18-micelles, respectively. As a reference, the decay rate constant, η, is 1.24 h^{-1} for DSPE-PEG micelles. Thus, both C16- and C18-micelles have fairly high stability, with C18-micelles being slightly better. The overall good kinetic stability can be attributed to the unique headgroup design where the 3-helix bundle positions compressed PEG chains to impart entropic repulsion to achieve superior stability relative to DSPE-PEG micelles.[28] However, it is worthwhile to note that the higher value of η for C16-micelles as compared with C18-micelles indicates that the alkyl chains also have some, although not drastic, effect on the *in vitro* stability of micelles although the alkyl chains were in a molten state.

These studies show that the subunit exchange from C18-micelles is slightly smaller relative to C16-micelles. Previous studies with DSPE-PEG micelles showed significant micelle stabilization when the temperature was below the melting temperature of alkyl chain in the micelle core.[39] In our case, the physiological temperature is well above the transition temperatures of both C16- and C18-micelles, and hence the alkyl chains in the micelle core are in a disordered/molten state. Greater hydrophobicity of C18 alkyl tails would result in larger intermolecular interactions between alkyl tails in the core of C18-micelles that would lead to slower subunit exchange. From a thermodynamic perspective, the physical state of alkyl chains in the molten micelle core would also affect micelle stability at a given temperature. The further the temperature is from the melting transition, the more "liquid" like the chains would be, with higher mobility. Hence, the activation barrier for subunit exchange would be inversely related to the difference in temperature of the experiment and transition temperature measured by DSC, as given by (37 °C − T_m). The smaller temperature difference (37 °C − T_m) for the C18-micelle and
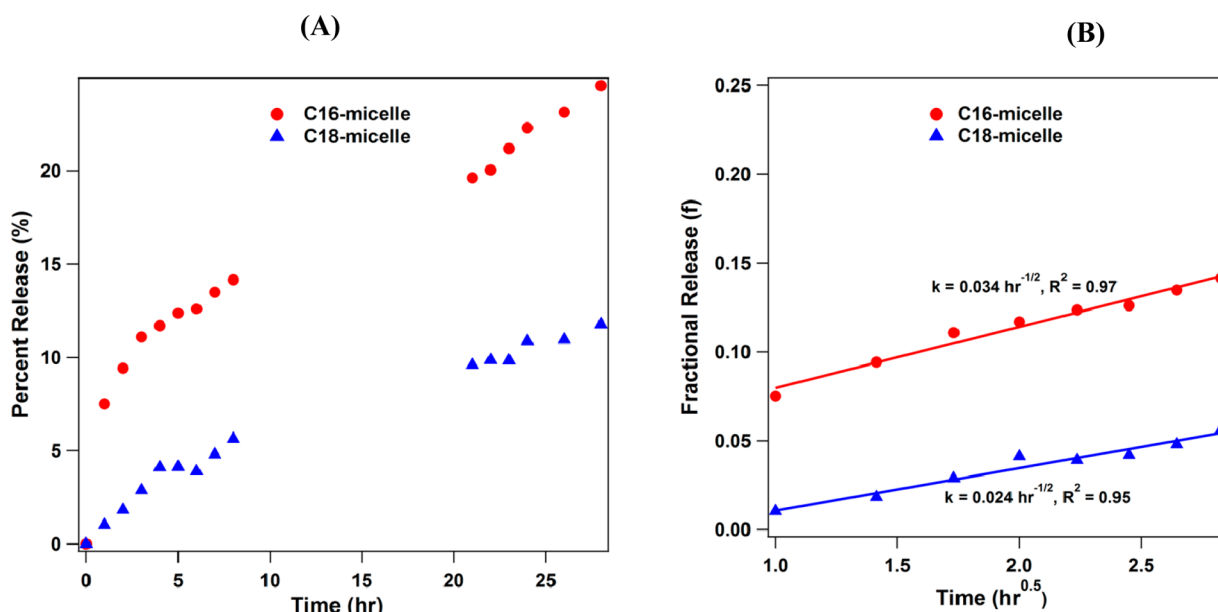
Figure 4. (A) Release profile of DOX from C16- and C18-micelles. Drug loaded micelle solutions (3 mg/mL, 2 mL) were placed in dialysis bags with MWCO 3500 Da, and release was monitored by quantification of drug in micelles at different times as determined by HPLC. (B) Fits of DOX release to Higuchi model for diffusive release. Solid lines show the fits of the data to Higuchi equation, given by $f = kt^{0.5}$, where f is fractional drug release, t is time, and k is Higuchi constant. The values of k obtained by fits are 0.024 $h^{-1/2}$ for C16-micelles, and 0.034 $h^{-1/2}$ for C18-micelles.

more hydrophobic C18 chains lead to slower subunit kinetics and result in their higher stability relative to C16-micelles.

The effect of the alkyl tail on cargo loading and cargo release kinetics from 3-helix micelles was quantified using DOX as a model drug. The DOX loading was 7.3 ± 0.5 wt % in C16-micelles, and 7.8 ± 0.4 wt % in C18-micelles. The size, uniformity of size distribution, and aqueous solubility of both micelles were maintained after DOX incorporation. Quantification of drug release by the dialysis technique shows sustained release from both micelles (Figure 4A). For C16-micelles, ∼8% of DOX is released within 1 h, followed by ∼22% after 24 h, whereas only 1% DOX is released from C18-micelles within the initial first hour, followed by ∼10% at 24 h. The release of DOX from both micelles is comparable to optimized block copolymer formulations that exhibit DOX release in the range of 20−40% after 24 h.[42−44] In the absence of degradation and swelling of micelles, DOX release could be fit to the Higuchi model based on diffusive release with reasonable accuracy (Figure 4B). The Higuchi rate constants obtained from linear fits are 0.034 $h^{-1/2}$ for DOX release from C16-micelles and 0.024 $h^{-1/2}$ from C18-micelles, which correspond to diffusion constants of 1.57 × 10^{-20} and 7.85 × 10^{-21} cm^2/s, respectively. Diffusion constants in the range of 10^{-15}−10^{-18} cm^2/s have been reported for the release of variety of cargo molecules from block copolymer micelles.[45,46] The core hydrophobicity affects the micelle stability, micelle−drug interactions, and thus the rate of drug release. The diffusion constants for DOX release from both micelles are significantly smaller, which suggests small drug leakage from 3-helix micelles. Again, this can be attributed to the overall stability of 3-helix micelle originating from the unique headgroup design. However, it is worthwhile to note that the diffusion constant of DOX from C18-micelles is an order of magnitude lower than that from C16-micelles.

The observed differences between the two micelles in terms of *in vitro* stability are small, and it is important to quantify the extent of difference in their *in vivo* stability to establish the design principles of 3-helix micelles for various biological

applications. The *in vivo* stability of C16-micelles in mice was assessed by PET in the present study and compared to that of C18-micelles reported previously.[18] ^{64}Cu-labeled micelles were intravenously administered to mice bearing NDL tumors. PET images in Figure 5 depict the differences in the accumulation
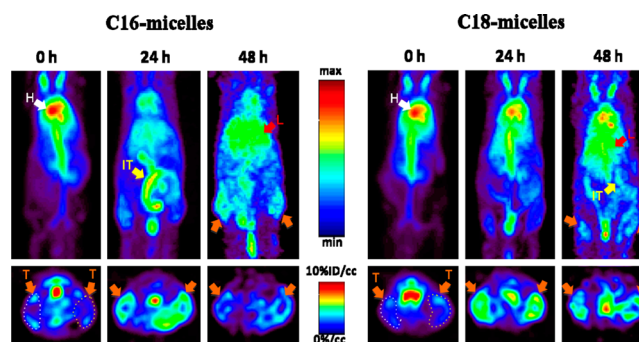

Figure 5. Evaluation of *in vivo* micelle stability by positron emission tomography (PET). The images acquired at 0, 24, and 48 h are presented. Top row: projection PET images after the intravenous administration of ^{64}Cu-labeled C16- and C18-micelles through the tail vein in mice. Lower row: transverse view of PET images. Arrows shown indicate the tumor (T, orange), heart (H, white), liver (L, red), and intestinal tract (IT, yellow).

and clearance of radioactivity between C16- and C18-micelles. Projected whole body images show that the radioactivity from C16-micelles is cleared from the blood pool and secreted through the intestinal tract faster than that of C18-micelles (Figure 5). The absorbed C-16 micelles in liver can dissociate and are rapidly secreted with biliary phosphatidylcholine as previously reported.[47] The time activity curve of the radiolabeled micelles in blood shows that the radioactivity of C16-micelles at 24 (12.03 ± 0.32% ID/cc) and 48 h (5.81 ± 0.23% ID/cc) is significantly lower than that of C18-micelles at 24 (25.74 ± 1.77% ID/cc, p < 0.0001) and 48 h (15.17 ± 1.58%
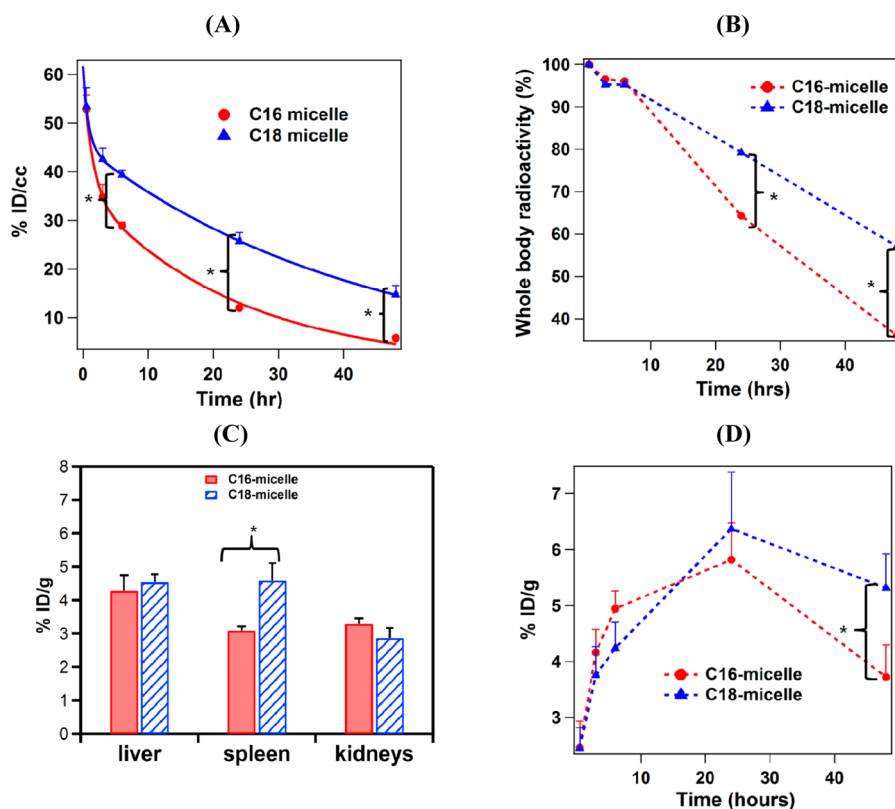
(A)

(B)

(C)

(D)

Figure 6. Quantitative analysis of PET images and biodistribution. (A) Blood radioactivity (%ID/cc) of ^{64}Cu-labeled C16- and C18-micelles. Curves were fit as two-phase exponential decay. For C16-micelles, the fit is given by $Y = 36.61e^{-0.043t} + 24.73e^{-0.74t}$, with $t_{1/2,\beta} = 16.12$ h; and for C18-micelles, the fit is given by $Y = 45.32e^{-0.0235t} + 16.42e^{-1.27t}$, with $t_{1/2,\beta} = 29.52$ h. (B) Whole body radioactivity (normalized by initial value as 100%) of ^{64}Cu-labeled C16- and C18-micelles. (C) Biodistribution (%ID/g) of C16- and C18-micelles in major clearance organs. (D) Tumor accumulation of micelles as a function of time shows that C18-micelles have significantly higher extent of tumor localization, 48 h after intravenous administration ($p < 0.0001$). Statistical significance was determined by t tests (unpaired) corrected for multiple comparisons using the Holm-Sidak method, with $\alpha = 5\%$.

ID/cc, $p < 0.0001$) (Figure 6A). The whole body radioactivity from C16-micelles at 24 ($p < 0.0001$) and 48 h ($p < 0.0001$) is reduced significantly compared to C18-micelles (Figure 6B). The β-phase blood circulation half-life ($t_{1/2,\beta}$) of C16-micelles, fit to a biphasic model, is 16.1 h, lower than that of C18-micelles (29.5 h), as reported previously.[18] These results demonstrated higher *in vivo* stability of C18-micelles, with extended blood circulation. The difference in blood circulation time between the two micelles is larger than that shown by the *in vitro* stability (Figure 3) and drug release kinetics (Figure 4). The radioactivity observed for ^{64}Cu-labeled C16-micelles, 48 h after injection, is 3.1 ± 0.3% ID/g in the spleen, 4.3 ± 0.5% ID/g in the liver, and 3.3 ± 0.1% ID/g in the kidney. The accumulation of C18-micelles was similar in the liver and kidney, but the spleen radioactivity of C16-micelles ($p < 0.001$) was lower than that reported previously for C18-micelles (Figure 6C).

The greatest differences in biodistribution between the C16- and C18-micelle are in the tumor accumulation at 48 h after injection. Transverse PET images (Figure 5) show that both micelles accumulate in tumor, 24 h after administration. Figure 6D plots the accumulation of the two micelles in the tumor tissue as a function of time. At 48 h, the accumulation levels for C16- and C18-micelles are 3.7 ± 0.5% ID/g and 5.3 ± 0.6% ID/g, respectively. The significantly higher activity from C18-micelles ($p < 0.0001$) is consistent with their longer blood circulation time that led to greater tumor accumulation. These

results are consistent with earlier studies that have shown increased tumor uptake for nanocarriers with enhanced blood circulation leading to more efficient passive targeting of the tumor tissue.[30,31] This amplification of the difference in the *in vivo* stability and extent of tumor accumulation between C16- and C18-micelles underscores the importance of the alkyl chain length and hydrophobicity in the micelle design on their pharmacokinetics.

The unique design of the 3-helix micelle shell based on PEG conjugates of coiled-coil 3-helix bundles provides high stability as compared to other nanocarriers in a similar size range. In previous studies, we have established the importance of the tertiary structure of the amphiphile headgroup on directional repulsion between PEG chains that leads to high stability of 3-helix micelles. The focus of this study is to delineate and quantify the contribution from the core forming alkyl tails to 3-helix micelle stability. Amphiphiles with C16 and C18 alkyl tails form well-defined core−shell micelles, with uniform size distribution as confirmed by DLS and SAXS measurements. The alkyl tails in core of 3-helix micelles exhibit an endothermic phase transition, with transition temperatures of 15 and 24 °C for C16- and C18-micelles, respectively. C18-micelles exhibit higher stability with a slower rate of subunit exchange, relative to C16-micelles, in the presence of serum proteins at 37 °C. The slower rate of DOX release from C18 micelles is in agreement with their higher stability. Evaluation of pharmacokinetics of radiolabeled C16- and C18-micelles by PET imaging

shows significantly longer blood circulation of C18-micelles with half-life of 29.5 h, compared to 16.1 h for C16-micelles. The differences between the two micelles in terms of their *in vivo* circulation stability are more pronounced compared to the differences in terms of *in vitro* stability and cargo release kinetics. We speculate that the complex biological environment in circulation including dynamic blood flow conditions and the presence of a large number of proteins that act as traps for amphiphilic assemblies have a critical impact on the distinction between pharmacokinetics of injected carriers. These studies underscore the significance of the thermal characteristics of core forming alkyl chains on stability of 3-helix micelles in conditions relevant to intravenous administration. Higher transition temperature for melting of C18 chains, combined with their higher hydrophobicity and lower mobility at physiological temperature result in higher *in vivo* stability of C18-micelles with longer blood circulation time and greater extent of tumor accumulation. These results indicate that 3-helix micelles based on C18 alkyl tails would be highly promising for intravenous drug delivery intended for cancer therapeutics. This systematic study allows comprehension of the contribution of tail length on 3-helix micelle stability, separately from the micelle headgroup. The results of this study serve as important guidelines to determine the suitability of nanocarriers based on 3-helix micelles with tunable *in vivo* circulation times intended for different biological applications.

CONCLUSION

In summary, we present a systematic investigation of the effect of alkyl chain length on size, core packing, *in vitro* stability, cargo release kinetics, and pharmacokinetics of 3-helix micelles. The present studies clearly show that the core forming alkyl chains are an equally important design parameter that could be used to tailor the stability and *in vivo* behavior of 3-helix micelles. Enthalpy of the alkyl chain phase transition in C18-micelles is higher compared to that in C16-micelles, consistent with higher hydrophobic interactions between C18 chains. C18-micelles exhibit higher stability with a slower rate of subunit exchange, relative to C16-micelles, in the presence of serum proteins at 37 °C. C18-micelles show slower and extended cargo release compared to C16-micelles. The diffusion constant for DOX release from C18-micelles is approximately half of that from C16-micelles, in agreement with their higher stability. The difference between the two micelles in terms of their *in vivo* circulation stability and extent of tumor accumulation are more pronounced compared to the differences in the *in vitro* stability and cargo release kinetics. The results from this study underscore the significance of choice of alkyl tails on the stability of 3-helix micelles in complex biological environments.

ASSOCIATED CONTENT

Ⓢ Supporting Information

Structural characterization of 3-helix micelles with C16 and C18 alkyl chains is provided. This material is available free of charge via the Internet at http://pubs.acs.org.

AUTHOR INFORMATION

Corresponding Author

*E-mail: tingxu@berkeley.edu. Phone: 510-642-1632. Fax: 510-643-5792.

Author Contributions

Nikhil Dube and Jai W. Seo contributed equally.

Notes

The authors declare no competing financial interest.

REFERENCES

(1) Kazunori, K.; Glenn S, K.; Masayuki, Y.; Teruo, O.; Yasuhisa, S. *J. Controlled Release* **1993**, *24*, 119−132.
(2) Kwon, G. S.; Kataoka, K. *Adv. Drug Delivery Rev.* **1995**, *16*, 295−309.
(3) Allen, C.; Maysinger, D.; Eisenberg, A. *Colloids Surf., B* **1999**, *16*, 3−27.
(4) Kataoka, K.; Matsumoto, T.; Yokoyama, M.; Okano, T.; Sakurai, Y.; Fukushima, S.; Okamoto, K.; Kwon, G. S. *J. Controlled Release* **2000**, *64*, 143−153.
(5) O'Reilly, R. K.; Hawker, C. J.; Wooley, K. L. *Chem. Soc. Rev.* **2006**, *35*, 1068−1083.
(6) Matsumura, Y. *Adv. Drug Delivery Rev.* **2008**, *60*, 899−914.
(7) Matsumura, Y.; Kataoka, K. *Cancer Sci.* **2009**, *100*, 572−579.
(8) Peters, D.; Kastantin, M.; Kotamraju, V. R.; Karmali, P. P.; Gujraty, K.; Tirrell, M.; Ruoslahti, E. *Proc. Natl. Acad. Sci. U.S.A.* **2009**, *106*, 9815−9819.
(9) Ebrahim Attia, A. B.; Ong, Z. Y.; Hedrick, J. L.; Lee, P. P.; Ee, P. L. R.; Hammond, P. T.; Yang, Y.-Y. *Curr. Opin. Colloid Interface Sci.* **2011**, *16*, 182−194.
(10) Lu, J.; Owen, S. C.; Shoichet, M. S. *Macromolecules* **2011**, *44*, 6002−6008.
(11) Elsabahy, M.; Wooley, K. L. *Chem. Soc. Rev.* **2012**, *41*, 2545−2561.
(12) Owen, S. C.; Chan, D. P. Y.; Shoichet, M. S. *Nano Today* **2012**, *7*, 53−65.
(13) Rösler, A.; Vandermeulen, G. W. M.; Klok, H.-A. *Adv. Drug Delivery Rev.* **2012**, *64*, 270−279.
(14) Dube, N.; Shu, J. Y.; Dong, H.; Seo, J. W.; Ingham, E.; Kheirolomoom, A.; Chen, P.-Y.; Forsayeth, J.; Bankiewicz, K.; Ferrara, K. W.; Xu, T. *Biomacromolecules* **2013**, *14*, 3697−3705.
(15) Chen, H.; Kim, S.; He, W.; Wang, H.; Low, P. S.; Park, K.; Cheng, J.-X. *Langmuir* **2008**, *24*, 5213−5217.
(16) Chen, H.; Kim, S.; Li, L.; Wang, S.; Park, K.; Cheng, J.-X. *Proc. Natl. Acad. Sci. U.S.A.* **2008**, *105*, 6596−6601.
(17) Letchford, K.; Burt, H. M. *Mol. Pharm.* **2011**, *9*, 248−260.
(18) Dong, H.; Dube, N.; Shu, J. Y.; Seo, J. W.; Mahakian, L. M.; Ferrara, K. W.; Xu, T. *ACS Nano* **2012**, *6*, 5320−5329.
(19) Allen, C.; Yu, Y.; Maysinger, D.; Eisenberg, A. *Bioconjugate Chem.* **1998**, *9*, 564−572.
(20) Jette, K.; Law, D.; Schmitt, E.; Kwon, G. *Pharm. Res.* **2004**, *21*, 1184−1191.
(21) Adams, M. L.; Kwon, G. S. *J. Biomater. Sci.* **2002**, *13*, 991−1006.
(22) Yamamoto, Y.; Yasugi, K.; Harada, A.; Nagasaki, Y.; Kataoka, K. *J. Controlled Release* **2002**, *82*, 359−371.
(23) Sun, X.; Rossin, R.; Turner, J. L.; Becker, M. L.; Joralemon, M. J.; Welch, M. J.; Wooley, K. L. *Biomacromolecules* **2005**, *6*, 2541−2554.
(24) Diezi, T. A.; Bae, Y.; Kwon, G. S. *Mol. Pharmaceutics* **2010**, *7*, 1355−1360.
(25) Zhao, X.; Poon, Z.; Engler, A. C.; Bonner, D. K.; Hammond, P. T. *Biomacromolecules* **2012**, *13*, 1315−1322.

(26) Perrault, S. D.; Walkey, C.; Jennings, T.; Fischer, H. C.; Chan, W. C. W. *Nano Lett.* **2009**, *9*, 1909−1915.

(27) Popović, Z.; Liu, W.; Chauhan, V. P.; Lee, J.; Wong, C.; Greytak, A. B.; Insin, N.; Nocera, D. G.; Fukumura, D.; Jain, R. K.; Bawendi, M. G. *Angew. Chem., Int. Ed.* **2010**, *49*, 8649−8652.

(28) Dong, H.; Shu, J. Y.; Dube, N.; Ma, Y.; Tirrell, M. V.; Downing, K. H.; Xu, T. *J. Am. Chem. Soc.* **2012**, *134*, 11807−11814.

(29) Zinn, T.; Willner, L.; Lund, R.; Pipich, V.; Richter, D. *Soft Matter* **2012**, *8*, 623−626.

(30) Gillies, E. R.; Dy, E.; Fréchet, J. M. J.; Szoka, F. C. *Mol. Pharmaceutics* **2005**, *2*, 129−138.

(31) Lee, C. C.; Gillies, E. R.; Fox, M. E.; Guillaudeu, S. J.; Fréchet, J. M. J.; Dy, E. E.; Szoka, F. C. *Proc. Natl. Acad. Sci. U.S.A.* **2006**, *103*, 16649−16654.

(32) Lim, J.; Guo, Y.; Rostollan, C. L.; Stanfield, J.; Hsieh, J.-T.; Sun, X.; Simanek, E. E. *Mol. Pharmaceutics* **2008**, *5*, 540−547.

(33) Shu, J. Y.; Tan, C.; DeGrado, W. F.; Xu, T. *Biomacromolecules* **2008**, *9*, 2111−2117.

(34) Higuchi, W. I. *J. Pharm. Sci.* **1962**, *51*, 802−804.

(35) Miller, J. K.; Shattuck, D. L.; Ingalla, E. Q.; Yen, L.; Borowsky, A. D.; Young, L. J. T.; Cardiff, R. D.; Carraway, K. L.; Sweeney, C. *Cancer Res.* **2008**, *68*, 8286−8294.

(36) Ingalla, E. Q.; Miller, J. K.; Wald, J. H.; Workman, H. C.; Kaur, R. P.; Yen, L.; Fry, W. H. D.; Borowsky, A. D.; Young, L. J. T.; Sweeney, C.; Carraway, K. L. *J. Biol. Chem.* **2010**, *285*, 28691−28697.

(37) Fields, G. B.; Lauer, J. L.; Dori, Y.; Forns, P.; Yu, Y.-C.; Tirrell, M. *Pept. Sci.* **1998**, *47*, 143−151.

(38) Yu, Y.-C.; Tirrell, M.; Fields, G. B. *J. Am. Chem. Soc.* **1998**, *120*, 9979−9987.

(39) Kastantin, M.; Ananthanarayanan, B.; Karmali, P.; Ruoslahti, E.; Tirrell, M. *Langmuir* **2009**, *25*, 7279−7286.

(40) Ortiz, A.; Teruel, J. A.; Espuny, M. J.; Marqués, A.; Manresa, Á.; Aranda, F. J. *Int. J. Pharm.* **2006**, *325*, 99−107.

(41) Gore, T.; Dori, Y.; Talmon, Y.; Tirrell, M.; Bianco-Peled, H. *Langmuir* **2001**, *17*, 5352−5360.

(42) Kwon, G.; Naito, M.; Yokoyama, M.; Okano, T.; Sakurai, Y.; Kataoka, K. *J. Controlled Release* **1997**, *48*, 195−201.

(43) Nystrom, A. M.; Xu, Z.; Xu, J.; Taylor, S.; Nittis, T.; Stewart, S. A.; Leonard, J.; Wooley, K. L. *Chem. Commun.* **2008**, 3579−3581.

(44) Lin, L. Y.; Lee, N. S.; Zhu, J.; Nyström, A. M.; Pochan, D. J.; Dorshow, R. B.; Wooley, K. L. *J. Controlled Release* **2011**, *152*, 37−48.

(45) Teng, Y.; Morrison, M. E.; Munk, P.; Webber, S. E.; Procházka, K. *Macromolecules* **1998**, *31*, 3578−3587.

(46) Lim Soo, P.; Luo, L.; Maysinger, D.; Eisenberg, A. *Langmuir* **2002**, *18*, 9996−10004.

(47) Seo, J. W.; Qin, S. P.; Mahakian, L. M.; Watson, K. D.; Kheirolomoom, A.; Ferrara, K. W. *J. Controlled Release* **2011**, *151*, 28−34.